Dynamical deformation in heavy ion reactions and the characteristics of quasifission products

S. Q. Guo,[1] Y. Gao,[1,2,*] J. Q. Li,[1,3] and H. F. Zhang[1,†]
[1]*School of Nuclear Science and Technology, Lanzhou University, Lanzhou 730000, China*
[2]*School of Information Engineering, Hangzhou Dianzi University, Hangzhou 310018, China*
[3]*Institute of Modern Physics, Chinese Academy of Sciences, Lanzhou 730000, China*
(Received 21 May 2017; revised manuscript received 14 September 2017; published 26 October 2017)

The investigation of the characteristics of low-energy heavy ion reactions covering both fusion and quasifission is carried out within the dinuclear system (DNS) concept, which is developed to include the deformation variables of fragments in addition to the mass numbers of the fragments, so that the energy dissipation, nucleon exchange, and deformation evolutions of the colliding nuclei as well as their correlations are treated simultaneously, and the potential energy surface of the system is thus reaction-time dependent. The direct consequence of introducing the deformation of fragments as dynamical variables is that one must treat the orientation between the two deformed nuclei. This is solved by introducing a barrier function. It is found that the model can reproduce data about the mass, as well as the total kinetic energy and its dispersion, of the reaction products very well, revealing that the DNS model has a reasonable theoretical foundation and thus can reliably describe the reaction mechanism.

DOI: 10.1103/PhysRevC.96.044622

I. INTRODUCTION

So far, all superheavy nuclei up to $Z = 118$ synthesized in laboratories have been produced via heavy ion fusion reactions [1–12]. However, further synthesis becomes more and more difficult, and a better understanding of the synthesis mechanism is needed. It is known that the formed compound nucleus gives no information about the reaction mechanism. However, the mass distribution and the distribution of the total kinetic energy (TKE) of the quasifission products reveal some very important characteristics such as the reaction paths, the entrance channel effects, and shell effects, with the result that quasifission (QF) is the most important mechanism preventing the formation of superheavy nuclei in the fusion of heavy nuclei [13–16]. Theoretically QF and fusion processes are described by the dinuclear system (DNS) concept [17–23]. The DNS model was developed to describe the time evolution of the deformation of the two interacting nuclei [23] in addition to the process of the nucleon transfer, where the intrinsic properties of the nuclei couple with the collective diffusion variables in the master equation via the driving potential of the system. The TKE of the QF products and its distribution are critically dependent on the fragment deformation. One challenge is whether the successful description of the dynamical deformation can correctly describe the TKE distribution of the QF products. On this basis the characteristics of the QF reactions are studied, shedding some interesting light on the reaction mechanism, and revealing the reasonable foundation of the DNS.

II. THEORETICAL FRAMEWORK

Based on the DNS, the evaporation residue cross-section can be written as a sum over all partial waves J [24]:

$$\sigma_{\rm ER}(E_{\rm c.m.}) = \frac{\pi\hbar^2}{2\mu E_{\rm c.m.}}\sum_J (2J+1)T(E_{\rm c.m.},J) \times P_{\rm CN}(E_{\rm c.m.},J)W_{\rm sur}(E_{\rm c.m.},J), \quad (1)$$

where the penetration coefficient $T(E_{\rm c.m.},J)$ describes the probability of the colliding nuclei at the incident energy $E_{\rm c.m.}$ overcoming the potential barrier in the entrance channel to form a DNS. $P_{\rm CN}(E_{\rm c.m.},J)$ is the probability for the DNS to form a compound nucleus via nucleon transfer, and $W_{\rm sur}(E_{\rm c.m.},J)$ is the survival probability for the compound nucleus in the deexcitation process.

During the collisions, the two nuclei gradually get deformed due to strong nuclear and Coulomb interactions between them [25–27]. Such a system also evolves along two main degrees of freedom: the transfer of nucleons in the mass asymmetry coordinate $\eta = (A_1 - A_2)/(A_1 + A_2)$ between the nuclei in the excited system leading to the compound nuclear formation, and the variation of the internuclear distance r of the nuclei in the interaction potential leading to QF. The evolution of the system is described by the following master equation [23]:

$$\begin{aligned}\frac{dP(A_1,\beta_1,\beta_2,E_1,t)}{dt} &= \sum_{A_1'} W_{A_1,\beta_1,\beta_2,E_1;A_1',\beta_1,\beta_2,E_1'}(t)[d_{A_1,\beta_1,\beta_2,E_1} \\ &\times P(A_1',\beta_1,\beta_2,E_1',t) - d_{A_1',\beta_1,\beta_2,E_1'}P(A_1,\beta_1,\beta_2,E_1,t)] \\ &+ \iint W_{A_1,\beta_1,\beta_2,E_1;A_1,\beta_1',\beta_2',E_1'}(t)[d_{A_1,\beta_1,\beta_2,E_1} \\ &\times P(A_1,\beta_1',\beta_2',E_1',t) - d_{A_1,\beta_1',\beta_2',E_1'}P(A_1,\beta_1,\beta_2,E_1,t)] \\ &\times \rho(\beta_1')\rho(\beta_2')d\beta_1'd\beta_2' \\ &- \Lambda^{qf}_{A_1,\beta_1,\beta_2,E_1}(\Theta(t))P(A_1,\beta_1,\beta_2,E_1,t), \end{aligned} \quad (2)$$

where $P(A_1,\beta_1,\beta_2,E_1,t)$ denotes the probability distribution function to find fragment 1 with A_1 nucleons, the quadrupole

*gaoyuan@impcas.ac.cn
†zhanghongfei@lzu.edu.cn

deformations of fragments being β_1, β_2 (here only the most important axially symmetric quadrupole deformations of the nuclei are considered, and always the tip-to-tip orientation is taken; afterwards it is remedied statistically), with the corresponding local excitation energy E_1 at time t, for the incident angular momentum J. β_1, β_2 are taken as two discrete variables, corresponding to the projectile-like and target-like fragments respectively. They are taken as continuous variables in the second line of Eq. (2); however, $\rho(\beta_i') = \frac{1}{h_i}$ is the density of discrete points with step length h_i $(i = 1,2)$. The local excitation energy E_1 is determined by the dissipated energy from the relative motion and the potential energy surface of the corresponding DNS [this will be shown later in Eqs. (8) and (9)]. The dissipation energy is described by the parametrization method of the classical deflection function [28–32]. $W_{A_1,\beta_1,\beta_2,E_1;A_1',\beta_1,\beta_2,E_1'}(t) = W_{A_1',\beta_1,\beta_2,E_1';A_1,\beta_1,\beta_2,E_1}(t)$ is the mean transition probability from channel $(A_1,\beta_1,\beta_2,E_1)$ to $(A_1',\beta_1,\beta_2,E_1')$. $d_{A_1,\beta_1,\beta_2,E_1}$ denotes the dimension corresponding to the macroscopic state $(A_1,\beta_1,\beta_2,E_1)$. The sum is taken over all possible mass numbers that a fragment A_1' may take, but only one-nucleon transfer is considered. The initial condition of Eq. (2) is $P(A_P,\beta_P,\beta_T,E_1 = 0,t = 0) = 1$, with the A_P and β_P,β_T being the mass number of the projectile and the ground state quadrupole deformations of projectile and target in the injection channel.

In this DNS, the fusion process to form the compound nucleus is competing with the QF, which can be described by incorporating the Kramers formula into Eq. (2) [33,34]. It is proved that the Kramers formula works well in the mass asymmetry region, where the QF barriers are relatively high [22]. The QF rate $\Lambda^{\rm qf}_{A_1,\beta_1,\beta_2,E_1}(\Theta(t))$ is estimated with the Kramers formula:

$$\Lambda^{\rm qf}_{A_1,\beta_1,\beta_2,E_1}(\Theta(t)) = \frac{\omega}{2\pi\omega^{B_{\rm qf}}}\left(\sqrt{\left(\frac{\Gamma}{2\hbar}\right)^2 + (\omega^{B_{\rm qf}})^2} - \frac{\Gamma}{2\hbar}\right) \times \exp\left(-\frac{B_{\rm qf}(A_1,\beta_1,\beta_2,E_1)}{\Theta(t)}\right). \quad (3)$$

The potential $V_{\rm CN}(r)$ of each DNS as a function of the internuclear distance r of the nuclei leading to QF is evaluated by using a double-folding method to calculate the nuclear and Coulomb interactions between two deformed nuclei with arbitrary orientation. A simplified Skryme-type interaction is adopted [35]. It is shown in Fig. 1 that the QF barrier $B_{\rm qf}$ is the depth of the pocket of the interaction potential. The local temperature is given by the Fermi-gas expression $\Theta = \sqrt{\varepsilon^*/a}$ with the level density parameter $a = A/12$ MeV^{-1} and the local excitation energy ε^*. The frequency $\omega^{B_{\rm qf}}$ is the frequency of the inverted harmonic oscillator approximating the interaction potential of two nuclei along the internuclear distance around the top of the quasifission barrier, and ω is the frequency of the harmonic oscillator approximating the potential along the internuclear distance around the bottom of the pocket. The quantity Γ denotes the double average width of the contributing single-particle states. Here constant values $\Gamma = 2.8$ MeV, $\hbar\omega^{B_{\rm qf}} = 2.0$ MeV, and $\hbar\omega = 3.0$ MeV were used. Then the QF yields as a function of the fragment

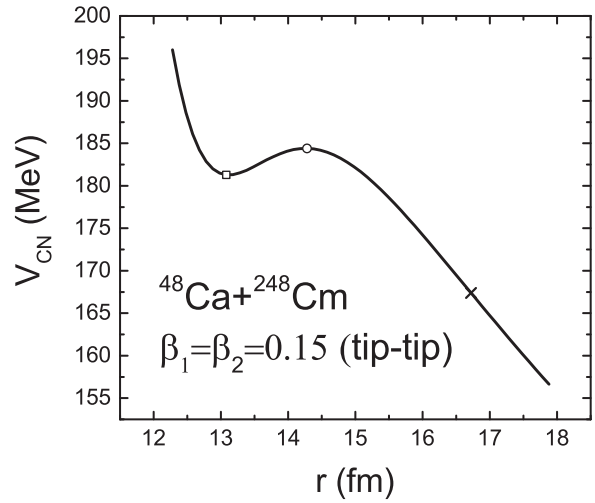

FIG. 1. The potential of each DNS as a function of the internuclear distance r of the nuclei leading to QF.

deformations are

$$Y_{\rm qf}(A_1,\beta_1,\beta_2,E_1) = \int_{t=0}^{\tau_{\rm int}} \Lambda^{\rm qf}_{A_1,\beta_1,\beta_2,E_1}(\Theta(t))P(A_1,\beta_1,\beta_2,E_1,t)dt. \quad (4)$$

The fusion probability is

$$P_{\rm CN} = \sum_{A_1=1}^{A_{\rm BG}} \iint P(A_1,\beta_1,\beta_2,\tau_{\rm int})\rho(\beta_1)\rho(\beta_2)d\beta_1 d\beta_2. \quad (5)$$

The interaction time $\tau_{\rm int}$ in the dissipative process of two colliding nuclei is dependent on the incident energy $E_{c.m.}$ and the incident angular momentum J, which is determined by using the deflection function method [29,31,32]. Hereafter we restrict ourselves to the study of the quasifission characteristics.

The potential energy surface (the driving potential for the nucleon transfer and the deformation evolution) of the DNS is

$$U(A_1,A_2,R,\beta_1,\beta_2,J) = E(A_1,\beta_1) + E(A_2,\beta_2) - \left[E(A_{\rm CN},\beta_{\rm CN}) + V^{\rm CN}_{\rm rot}(J)\right] + V_{\rm CN}(A_1,A_2,R,\beta_1,\beta_2,J), \quad (6)$$

where $A_{\rm CN} = A_1 + A_2$ is the mass number of the compound nucleus, R is the distance between nuclei at which the interaction potential between the two nuclei, $V_{\rm CN}(A_1,A_2,R,\beta_1,\beta_2,J)$, has the minimum value. $E(A_i,\beta_i)$ $(i = 1,2)$ and $E(A_{\rm CN},\beta_{\rm CN})$ are the total energies of the ith nucleus and the compound nucleus, respectively, in which the shell and the pairing corrections are included. They can be calculated as a sum of the liquid drop energy and the Strutinsky shell correction. We use the formula and parameters of Ref. [36]:

$$E(A_i,\beta_{i2}) = E_{\rm LD}(A_i)\left(1 + b_{i2}\beta_{i2}^2\right) + c_1 E_{\rm shell}(A_i,\beta_{i2}). \quad (7)$$

In the following, the notation $\beta_{i2} \equiv \beta_i$, and we take $b_2 = 0.0074A^{1/3} - 0.38A^{-1/3}$. The energy of a nucleus with respect to the axial deformations is calculated with a Skyrme energy-density functional together with the extended Thomas-Fermi

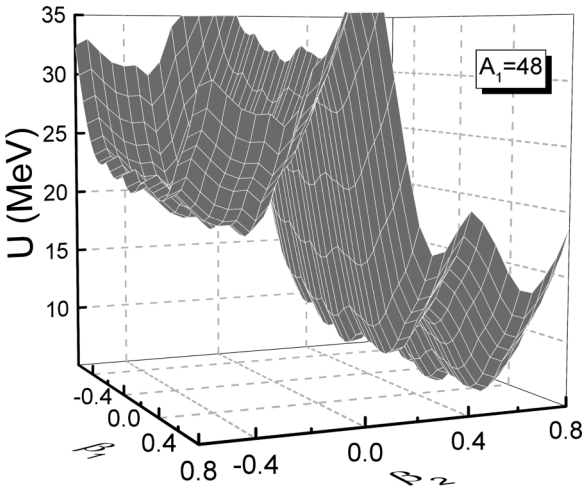

FIG. 2. The potential energy surface for the reaction ^{48}Ca + ^{248}Cm, which drives the nucleon transfer, and the deformation evolution, as a function of quadrupole deformations in the entrance channel ($A_1 = 48$).

approximation, which gives the minimum total energies of the ith nucleus with the optimum β_{i2}. The $V_{\rm rot}^{\rm CN}$ is the rotational energy of the compound nucleus. The interaction potential between the two nuclei $V_{\rm CN}(A_1,A_2,R,\beta_1,\beta_2,J)$ includes the nuclear, Coulomb interaction, and centrifugal parts. Here again a double-folding method is used to calculate the nuclear and Coulomb interaction between two deformed nuclei with arbitrary orientation. A simplified Skryme-type interaction is adopted. The details are given in Refs. [35,37]. The driving potential for the nucleon transfer and the deformation evolution is shown in Fig. 2.

In the relaxation process of the relative motion, the DNS will be excited by the dissipation of the relative kinetic energy. The excited system opens a valence space $\Delta\varepsilon_K$ in each fragment K ($K = 1,2$), which has a symmetrical distribution around the Fermi surface. Only the particles in the states within this valence space are actively involved in the excitation and transfer [38]:

$$\Delta\varepsilon_K = \sqrt{\frac{4\varepsilon_K^*}{g_K}}, \quad \varepsilon_K^* = \varepsilon^* \frac{A_K}{A}, \quad g_K = \frac{A_K}{12}, \tag{8}$$

where ε^* is the local excitation energy of the DNS, which provides the excitation energy for the mean transition probability, so that the E_1 in Eq. (2) is determined as $E_1 = \varepsilon^*$. There are $N_K = g_K \Delta\varepsilon_K$ valence states and $m_K = N_K/2$ valence nucleons in the valence space $\Delta\varepsilon_K$, which gives the dimension $d(m_1,m_2) = \binom{N_1}{m_1}\binom{N_2}{m_2}$. The local excitation energy is defined as

$$\varepsilon^* = E_x - U(A_1,A_2,R,\beta_1,\beta_2,J). \tag{9}$$

The excitation energy E_x of the composite system is converted from the relative kinetic energy loss, which is related to the Coulomb barrier [37] and is determined for each initial relative angular momentum J by the parametrization method of the classical deflection function [28,30,32]. So, E_x is coupled with the relative angular momentum.

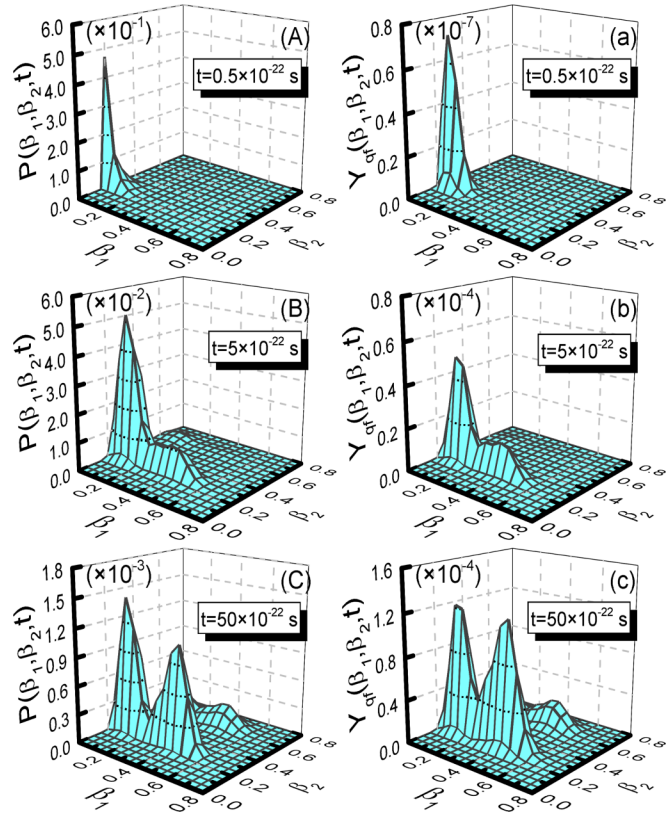

FIG. 3. The evolution of the distribution function $P(A_1,\beta_1,\beta_2,t)$ (left) and the mass yield $Y_{\rm qf}(A_1,\beta_1,\beta_2,t)$ (right) as a function of the fragment deformations of the reaction ^{48}Ca + ^{248}Cm for $A_1 = 48$.

III. RESULTS AND DISCUSSIONS

Under the potential energy surface, the master equation (2) is solved to obtain the probability distribution function $P(A_1,\beta_1,\beta_2,E_1,t)$ with A_1 nucleons in fragment 1, and the quadrupole deformations of fragments are β_1, β_2 at the time t. It displays the evolution of the distribution function for $A_1 = 48$ at different time as indicated in the Fig. 3 (left). At the initial stage of the reaction up to $t = 0.5 \times 10^{-22}$ s the probability function is distributed around the injection point with $\beta_P = 0.0$ and $\beta_T = 0.235$. With increasing time it diffuses, becoming distributed into a wider area with wider nuclear deformations. At $t = 50 \times 10^{-22}$ s an appreciable probability is accumulated at the several places. Because nuclei have different deformations, their shell correction energies are different. The large shell correction energy is the reason that the distribution functions are localized in these places.

For the whole process, our dynamical calculation shows that it evolves in a manner quite different from a Gaussian distribution [34]. Figure 3 (right) displays the evolution of the the mass yield distribution $Y_{\rm qf}(A_1,\beta_1,\beta_2,t)$ with $A_1 = 48$. At each time it looks very much like the distribution function $P(A_1,\beta_1,\beta_2,E_1,t)$, indicating that in Eq. (4) the distribution probability plays the dominant role.

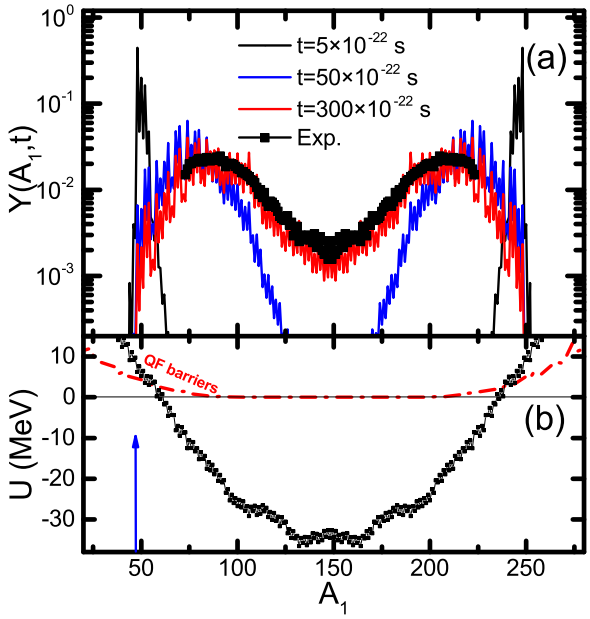

FIG. 4. (a) The evolution of the relative quasifission yield distribution $Y(A_1)$ of the reaction ^{48}Ca + ^{248}Cm at $E_{\rm c.m.} = 205$ MeV. The data are taken from Ref. [15]. (b) The energy surface as a function of A_1, with β_1 and β_2 being the values at which the energy surface is the lowest. The arrow in the figure indicates the injection channel.

The mass distribution of the QF products reads

$$Y_{\rm qf}(A_1) = \int_{t=0}^{\tau_{\rm int}} dt \int \rho(\beta_1) d\beta_1 \int \rho(\beta_2) d\beta_2 \times P(A_1,\beta_1,\beta_2,E_1,t)\Lambda^{\rm qf}_{A_1,\beta_1,\beta_2,E_1}(\Theta(t)). \quad (10)$$

Figure 4(a) shows the relative mass yield of QF products as a function of the fragment mass number A_1, normalized over the whole mass range to 200%, for the reaction ^{48}Ca + ^{248}Cm at different reaction times. As indicated in the figure, at the beginning of the reaction, $t = 5 \times 10^{-22}$ s, the yield is distributed near the injection point: $A_1 = 48$ and $A_2 = 248$. At $t = 50 \times 10^{-22}$ s, the dispersion area is enlarged and moves towards the mass-symmetric region. Finally, at $t = 300 \times 10^{-22}$ s, the dispersion tends to fit the experimental data. Black squares indicate the experimental data, which show two symmetric parabola-like peaks. The potential energy surface as a function of A_1 is shown in Fig. 4(b). For each A_1, the deformations of the nuclei β_1 and β_2 take values at which the energy surface is the lowest. One may see that the energy surface is getting very low in the symmetric region, which is in favor of mass distribution probability $P(A_1)$ accumulation. In the figure, the dash-dotted line denotes the quasifission barriers $B_{\rm qf}$. Note that on the left side the values are nearly zero from $A_1 = 100$ to $A_1 = 150$; this is in favor of the QF, i.e., the mass distribution probability $P(A_1)$ decreases faster. The consequence is that, with decreasing potential energy, the mass distribution probability $P(A_1)$ gains on one hand and loses on the other. So it first increases, reaches a maximum, then decreases. Since the QF yield mainly depends on $P(A_1)$, it correspondingly shows a maximum. The other side indicates the mass yield of the heavy fragment A_2. Further, at about $A_1 = 100$ and $A_1 = 200$ there are two minima in the energy potential, which will help to cause two maximum distributions of $P(A_1)$ and help maximum QF yields, and the position of the maximum may be influenced a little.

Based on the dynamical deformation, we now further calculate the mean total kinetic energy ⟨TKE⟩ of the QF products and its dispersion. The ⟨TKE⟩ of the QF fragments as a function of the light fragment mass number A_1 can be written as

$$\langle {\rm TKE}_{B(\beta_1,\beta_2)}(A_1)\rangle = \frac{\iint d\beta_1 d\beta_2 \rho(\beta_1)\rho(\beta_2){\rm TKE}_{B(\beta_1,\beta_2)}(A_1)Y_{\rm qf}(A_1,\beta_1,\beta_2)}{\iint d\beta_1 d\beta_2 \rho(\beta_1)\rho(\beta_2)Y_{\rm qf}(A_1,\beta_1,\beta_2)} \quad (11)$$

with ${\rm TKE}_{B(\beta_1,\beta_2)} = V_{\rm nucl}(R_b) + V_{\rm coul}(R_b)$, where the radius R_b is the position of the Coulomb barrier B in the tip-to-tip orientation; currently, it is taken as $R_b = 1.6[R_1(A_1,\beta_1) + R_2(A_2,\beta_2)]$ [40,41], which is actually the radius of the scission point. At the moment the orientation is not yet considered. Since the nuclei in each DNS under discussion are deformed, their different orientations will generate different Coulomb barriers,corresponding to different scission points, and therefore will generate different TKEs. For two deformed nuclei, they separate into the QF channel with all possible orientations, so all possible orientations must be taken into account. To simulate the orientation effect we use a barrier distribution function with a asymmetry Gaussian form. Suppose $B_0(\beta_1,\beta_2)$ and $B_s(\beta_1,\beta_2)$ are the height of the Coulomb barrier at waist-to-waist orientation and the height of the minimum barrier; the corresponding TKE will be ${\rm TKE}_{B_0(\beta_1,\beta_2)}$ and ${\rm TKE}_{B_s(\beta_1,\beta_2)}$, respectively. The barrier distribution function as a function of the barrier $B_X(\beta_1,\beta_2)$ [42–44] reads $f(B_X(\beta_1,\beta_2)) = \frac{1}{N}\exp[-(\frac{B_X(\beta_1,\beta_2)-B_m(\beta_1,\beta_2)}{\Delta_1})^2]$ $[B_X(\beta_1,\beta_2) < B_m(\beta_1,\beta_2)]$ and $f(B_X(\beta_1,\beta_2)) = \frac{1}{N}\exp[-(\frac{B_X(\beta_1,\beta_2)-B_m(\beta_1,\beta_2)}{\Delta_2})^2]$ $[B_X(\beta_1,\beta_2) > B_m(\beta_1,\beta_2)]$, with $B_m(\beta_1,\beta_2) = [B_0(\beta_1,\beta_2) + B_s(\beta_1,\beta_2)]/2$ and $\Delta_2 = [B_0(\beta_1,\beta_2) - B_s(\beta_1,\beta_2)]/2$. The value of Δ_1 is several MeV less than the value of Δ_2; usually it is taken as 2–4 MeV. By using the barrier function, the mean TKE and the variance of TKE become

$$\langle {\rm TKE}(A_1)\rangle = \frac{\iint d\beta_1 d\beta_2 \rho(\beta_1)\rho(\beta_2)\int dB_X(\beta_1,\beta_2) f(B_X(\beta_1,\beta_2)){\rm TKE}_{B_X(\beta_1,\beta_2)}(A_1)Y_{\rm qf}(A_1,\beta_1,\beta_2)}{\iint d\beta_1 d\beta_2 \rho(\beta_1)\rho(\beta_2)Y_{\rm qf}(A_1,\beta_1,\beta_2)}, \quad (12)$$

$$\sigma^2_{\rm TKE}(A_1) = \langle {\rm TKE}(A_1)^2\rangle - \langle {\rm TKE}(A_1)\rangle^2 = \frac{\iint d\beta_1 d\beta_2 \rho(\beta_1)\rho(\beta_2)\int dB_X(\beta_1,\beta_2) f(B_X(\beta_1,\beta_2))({\rm TKE}_{B_X(\beta_1,\beta_2)}(A_1))^2 Y_{\rm qf}(A_1,\beta_1,\beta_2)}{\iint d\beta_1 d\beta_2 \rho(\beta_1)\rho(\beta_2)Y_{\rm qf}(A_1,\beta_1,\beta_2)} - \langle {\rm TKE}(A_1)\rangle^2. \quad (13)$$

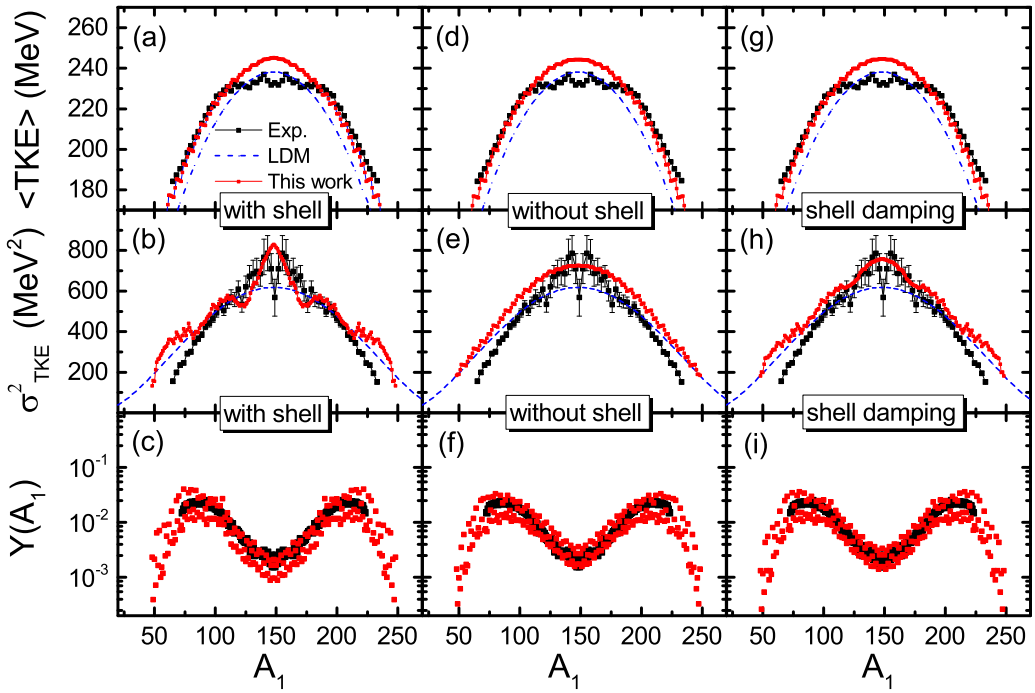

FIG. 5. The $\langle \mathrm{TKE}(A_1)\rangle$, the variance $\sigma^2_{\mathrm{TKE}}(A_1)$ of TKE, and the relative mass yield $Y(A_1)$ of the QF products in the reaction $^{48}\mathrm{Ca} + ^{248}\mathrm{Cm}$ at $E_{\mathrm{c.m.}} = 205$ MeV. The quantities in the left column are the ones calculated with the shell correction, those in the middle are calculated with the shell corrections being witched off, and those in the right column are calculated with the damped shell corrections. The blue dashed lines are the results obtained by LDM [39]. The experimental data are from Ref. [15].

The mean TKE, the variance of TKE, and the QF mass yield $Y(A_1)$ as a function of A_1 for the reaction $^{48}\mathrm{Ca} + ^{248}\mathrm{Cm}$ at $E_{\mathrm{c.m.}} = 205$ MeV are shown in Fig. 5 with and without the shell correction, and with the damped shell correction. For an excited nucleus, its shell correction energy will be damped due to the excitation energy. The excitation-energy-dependent shell correction energy in Eq. (7) is taken as $E_{\mathrm{shell}}(A_i,\beta_i,E_i) = E_{\mathrm{shell}}(A_i,\beta_i,E_i=0)\times\exp[-E_i/E_d]$, where the damping factor $E_d = 0.5A_i^{4/3}/a(A_i)$ with the level density parameter $a(A_i) = A_i/12\ \mathrm{MeV}^{-1}$ [45].

The red lines in the first row show that our calculated $\langle \mathrm{TKE}\rangle$ can basically follow the experimental data, and they are not influenced by the shell correction, since they are mainly dependent on the nuclear deformation. Our calculated $\sigma^2_{\mathrm{TKE}}(A_1)$ can also basically follow the data, only the $\sigma^2_{\mathrm{TKE}}(A_1)$ in panel (b) of Fig. 5 shows much too distinct oscillation; obviously it is due to the shell correction. When the shell correction is switched off, the curve becomes smooth, as shown in Fig. 5(e). When the excitation energy of the QF product is taken into account, so that the shell correction energy is damped, the agreement with the experimental data is greatly improved. One may see that, in the very symmetric mass region, the data for $\sigma^2_{\mathrm{TKE}}(A_1)$ are smaller. The experimental data includes the fragments from the compound nuclear fission, and they have no orientation problem; therefore they produce small TKE dispersion. As indicated in Fig. 6, in which the $\langle \mathrm{TKE}(A_1)\rangle$ and the variance $\sigma^2_{\mathrm{TKE}}(A_1)$ are calculated only for tip-to-tip orientation, one may find that the $\langle \mathrm{TKE}(A_1)\rangle$ can still follow the data if the scission is taken as $R_b = (1.4/r0)[R_1(A_1,\beta_1) + R_2(A_2,\beta_2)] + 1$ fm [40]. The top of the curve is not smooth due to the limited statistics. However, the $\sigma^2_{\mathrm{TKE}}(A_1)$ is significantly small, and cannot be improved unless the orientation has been taken into account. This indicate that the nuclear dynamical deformation and the

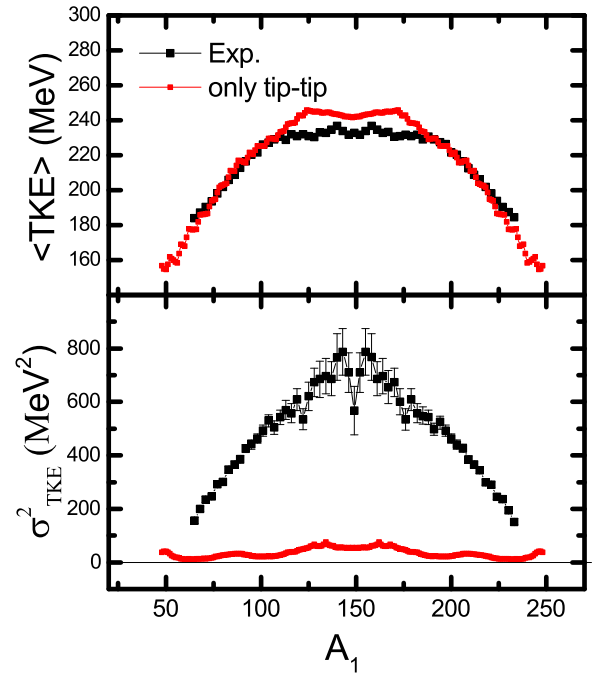

FIG. 6. $\langle \mathrm{TKE}(A_1)\rangle$, the variance $\sigma^2_{\mathrm{TKE}}(A_1)$ of QF fragments with only tip-tip orientation in the reaction $^{48}\mathrm{Ca} + ^{248}\mathrm{Cm}$ at $E_{\mathrm{c.m.}} = 205$ MeV. The black squares represent the experimental data from Ref. [15].

orientation of the two deformed nuclei are the origin of the large TKE fluctuation, which proves the existence of the two individual deformed nuclei; this is the very foundation of the DNS concept. Since the fluctuation of the TKE is symmetric to the mean TKE, the fluctuation does not change the behavior of the mean value. By considering the dynamical deformation, the calculated QF mass yield distribution $Y(A_1)$ agrees well with the data [15], and the shell correction does not influence it since the QF barrier plays a more important role (please see our explanation in Fig. 4).

IV. SUMMARY

To sum up, the fusion reactions leading to superheavy elements and to the QF products are successfully described by the DNS model. Although the QF products can shed more light on the reaction mechanism, the yields of the QF products alone does not provide thorough information. Therefore the distribution of the TKE of the QF products is measured and calculated. The kinetic energy of the QF products critically depends on the deformations of the QF products. By using our extended master equation, in which the deformations of the nuclei in the DNS are taken as dynamical valuables in addition to the project-like mass number, the mass transfer and the deformation evolutions of the fragments are described simultaneously. By further considering all relative orientation of the deformed two nuclei, the mean TKE and the variance of the TKE distribution are successfully described. This indicates that in the reaction process there really exist two deformed nuclei; their separation with different orientations generates a large fluctuation in the TKE of fragments. This strengthens the theoretical foundation of the DNS concept, though phenomenologically. By taking the deformations of the nuclei in the DNS to be dynamical valuables, the intrinsic properties of nuclei are thus coupled with the relative interaction, and the energy surface of the reaction system becomes time dependent. This is an important development for the diffusion, as well as for the reaction theory.

ACKNOWLEDGMENTS

The work is supported by the National Natural Science Foundation of China (Grants No. 11475050 and No. 11675066), by a Zhejiang Province Science and Technology Plan project (2015C33035), and by the Feitian Scholar Project of Gansu province. We appreciate very much very instructive discussions with Prof. Jingdong Bao and Prof. Jieding Zhu.

[1] S. Hofmann, Prog. Part. Nucl. Phys. **62**, 337 (2009).
[2] K. Morita, K. Morimoto, D. Kaji, T. Akiyama, S. ichi Goto, H. Haba, E. Ideguchi, R. Kanungo, K. Katori, H. Koura, H. Kudo, T. Ohnishi, A. Ozawa, T. Suda, K. Sueki, H. Xu, T. Yamaguchi, A. Yoneda, A. Yoshida, and Y. Zhao, J. Phys. Soc. Jpn. **73**, 2593 (2004).
[3] Y. Oganessian, J. Phys. G: Nucl. Part. Phys. **34**, R165 (2007).
[4] Y. T. Oganessian, F. S. Abdullin, P. D. Bailey, D. E. Benker, M. E. Bennett, S. N. Dmitriev, J. G. Ezold, J. H. Hamilton, R. A. Henderson, M. G. Itkis, Y. V. Lobanov, A. N. Mezentsev, K. J. Moody, S. L. Nelson, A. N. Polyakov, C. E. Porter, A. V. Ramayya, F. D. Riley, J. B. Roberto, M. A. Ryabinin, K. P. Rykaczewski, R. N. Sagaidak, D. A. Shaughnessy, I. V. Shirokovsky, M. A. Stoyer, V. G. Subbotin, R. Sudowe, A. M. Sukhov, Y. S. Tsyganov, V. K. Utyonkov, A. A. Voinov, G. K. Vostokin, and P. A. Wilk, Phys. Rev. Lett. **104**, 142502 (2010).
[5] P. Armbruster, Annu. Rev. Nucl. Part. Sci. **35**, 135 (1985).
[6] S. Hofmann, Rep. Prog. Phys. **61**, 639 (1998).
[7] S. Hofmann and G. Münzenberg, Rev. Mod. Phys. **72**, 733 (2000).
[8] S. Hofmann, F. Heßberger, D. Ackermann, G. Münzenberg, S. Antalic, P. Cagarda, B. Kindler, J. Kojouharova, M. Leino, B. Lommel *et al.*, Eur. Phys. J. A **14**, 147 (2002).
[9] Y. T. Oganessian, V. K. Utyonkov, Y. V. Lobanov, F. S. Abdullin, A. N. Polyakov, I. V. Shirokovsky, Y. S. Tsyganov, G. G. Gulbekian, S. L. Bogomolov, B. N. Gikal, A. N. Mezentsev, S. Iliev, V. G. Subbotin, A. M. Sukhov, G. V. Buklanov, K. Subotic, M. G. Itkis, K. J. Moody, J. F. Wild, N. J. Stoyer, M. A. Stoyer, and R. W. Lougheed, Phys. Rev. Lett. **83**, 3154 (1999).
[10] Y. T. Oganessian, A. Yeremin, A. Popeko, S. Bogomolov, G. Buklanov, M. Chelnokov, V. Chepigin, B. Gikal, V. Gorshkov, G. Gulbekian *et al.*, Nature (London) **400**, 242 (1999).
[11] G. Danilyan, A. Fedorov, A. Gagarski, F. Goennenwein, P. Jesinger, J. von Kalben, A. Koetzle, Y. I. Korobkina, I. Krasnoshchekova, M. Mutterer *et al.*, Phys. At. Nucl. **63**, 1671 (2000).
[12] Y. T. Oganessian, V. Utyonkov, Y. V. Lobanov, F. S. Abdullin, A. Polyakov, I. Shirokovsky, Y. S. Tsyganov, G. Gulbekian, S. Bogomolov, B. Gikal *et al.*, Phys. Rev. C **62**, 041604 (2000).
[13] E. Prokhorova, A. Bogachev, M. Itkis, I. Itkis, G. Knyazheva, N. Kondratiev, E. Kozulin, L. Krupa, Y. T. Oganessian, I. Pokrovsky *et al.*, Nucl. Phys. A **802**, 45 (2008).
[14] I. Itkis, E. Kozulin, M. Itkis, G. Knyazheva, A. Bogachev, E. Chernysheva, L. Krupa, Y. T. Oganessian, V. Zagrebaev, A. Y. Rusanov *et al.*, Phys. Rev. C **83**, 064613 (2011).
[15] E. Kozulin, G. Knyazheva, I. Itkis, M. Itkis, A. Bogachev, E. Chernysheva, L. Krupa, F. Hanappe, O. Dorvaux, L. Stuttgé *et al.*, Phys. Rev. C **90**, 054608 (2014).
[16] M. Itkis, E. Vardaci, I. Itkis, G. Knyazheva, and E. Kozulin, Nucl. Phys. A **944**, 204 (2015).
[17] N. Antonenko, E. Cherepanov, A. Nasirov, V. Permjakov, and V. Volkov, Phys. Lett. B **319**, 425 (1993).
[18] G. Adamian, N. Antonenko, W. Scheid, and V. Volkov, Nucl. Phys. A **633**, 409 (1998).
[19] G. Adamian, N. Antonenko, A. Diaz-Torres, and W. Scheid, Nucl. Phys. A **671**, 233 (2000).
[20] G. Adamian, N. Antonenko, and W. Scheid, Nucl. Phys. A **678**, 24 (2000).
[21] A. Diaz-Torres, G. Adamian, N. Antonenko, and W. Scheid, Phys. Lett. B **481**, 228 (2000).
[22] M. Huang, Z. Gan, X. Zhou, J. Li, and W. Scheid, Phys. Rev. C **82**, 044614 (2010).
[23] M. Huang, Z. Zhang, Z. Gan, X. Zhou, J. Li, and W. Scheid, Phys. Rev. C **84**, 064619 (2011).

[24] W. Li, N. Wang, F. Jia, H. Xu, W. Zuo, Q. Li, E. Zhao, J. Li, and W. Scheid, J. Phys. G: Nucl. Part. Phys. **32**, 1143 (2006).
[25] A. Diaz-Torres, Phys. Rev. C **69**, 021603 (2004).
[26] A. Diaz-Torres, Phys. Rev. C **74**, 064601 (2006).
[27] L. Yu, Z. Gan, Z. Zhang, H. Zhang, and J. Li, Phys. Lett. B **730**, 105 (2014).
[28] G. Wolschin and W. Nörenberg, Z. Phys. A **284**, 209 (1978).
[29] A. Merchant and W. Nörenberg, Z. Phys. A **308**, 315 (1982).
[30] J. Li, X. Tang, and G. Wolschin, Phys. Lett. B **105**, 107 (1981).
[31] J. Q. Li and G. Wolschin, Phys. Rev. C **27**, 590 (1983).
[32] C. Riedel, G. Wolschin, and W. Nörenberg, Z. Phys. A **290**, 47 (1979).
[33] A. Diaz-Torres, G. G. Adamian, N. V. Antonenko, and W. Scheid, Phys. Rev. C **64**, 024604 (2001).
[34] G. G. Adamian, N. V. Antonenko, and W. Scheid, Phys. Rev. C **68**, 034601 (2003).
[35] Q. Li, W. Zuo, W. Li, N. Wang, E. Zhao, J. Li, and W. Scheid, Eur. Phys. J. A **24**, 223 (2005).
[36] N. Wang, M. Liu, and X. Wu, Phys. Rev. C **81**, 044322 (2010).
[37] Z.-Q. Feng, G.-M. Jin, F. Fu, and J.-Q. Li, Chinese Phys. C **31**, 366 (2007).
[38] S. Ayik, B. Schürmann, and W. Nörenberg, Z. Phys. A **279**, 145 (1976).
[39] J. R. Nix and W. J. Swiatecki, Nucl. Phys. **71**, 1 (1965).
[40] V. Zagrebaev and W. Greiner, J. Phys. G: Nucl. Part. Phys. **34**, 1 (2006).
[41] Y. Zhao, I. Nishinaka, Y. Nagame, M. Tanikawa, K. Tsukada, S. Ichikawa, K. Sueki, Y. Oura, H. Ikezoe, S. Mitsuoka *et al.*, Phys. Rev. Lett. **82**, 3408 (1999).
[42] Z.-Q. Feng, G.-M. Jin, F. Fu, and J.-Q. Li, Nucl. Phys. A **771**, 50 (2006).
[43] V. I. Zagrebaev, Phys. Rev. C **64**, 034606 (2001).
[44] V. I. Zagrebaev, Phys. Rev. C **67**, 061601 (2003).
[45] G. G. Adamian, N. V. Antonenko, and W. Scheid, Phys. Rev. C **69**, 011601 (2004).